ADVANCED FUNCTIONAL MATERIALS
www.afm-journal.de

Screening Conductive MXenes for Lithium Polysulfide Adsorption

Geetha Valurouthu, Mikhail Shekhirev, Mark Anayee, Ruocun (John) Wang, Kyle Matthews, Tetiana Parker, Robert W. Lord, Danzhen Zhang, Alex Inman, Marley Downes, Chi Won Ahn, Vibha Kalra, Il-Kwon Oh, and Yury Gogotsi**

MXenes are promising passive components that enable lithium-sulfur batteries (LSBs) by effectively trapping lithium polysulfides (LiPSs) and facilitating surface-mediated redox reactions. Despite numerous studies highlighting the potential of MXenes in LSBs, there are no systematic studies of MXenes' composition influence on polysulfide adsorption, which is foundational to their applications in LSB. Here, a comprehensive investigation of LiPS adsorption on seven MXenes with varying chemistries (Ti_2CT_x, $Ti_3C_2T_x$, Ti_3CNT_x, $Mo_2TiC_2T_x$, V_2CT_x, Nb_2CT_x, and $Nb_4C_3T_x$), utilizing optical and analytical spectroscopic methods is performed. This work reports on the influence of polysulfide concentration, interaction time, and MXenes' chemistry (transition metal layer, carbide and carbonitride inner layer, surface terminations and structure) on the amount of adsorbed LiPSs and the adsorption mechanism. These findings reveal the formation of insoluble thiosulfate and polythionate complex species on the surfaces of all tested MXenes. Furthermore, the selective adsorption of lithium and sulfur, and the extent of conversion of the adsorbed species on MXenes varied based on their chemistry. For instance, Ti_2CT_x exhibits a strong tendency to adsorb lithium ions, while $Mo_2TiC_2T_x$ is effective in trapping sulfur by forming long-chain polythionates. The latter demonstrates a significant conversion of intermediate polysulfides into low-order species. This study offers valuable guidance for the informed selection of MXenes in various functional components benefiting the future development of high-performance LSBs.

1. Introduction

Despite advancements in Li-ion battery technology, limited energy density, natural resource sustainability, and supply chain concerns make Li-ion batteries unlikely the only solution to all energy storage challenges.[1] Lithium-sulfur batteries (LSBs) show significant promise as an alternative to Li-ion batteries due to their high theoretical energy density (2600 Wh kg^{-1}), natural abundance of sulfur, and environmental benignity.[2,3] Nonetheless, their development faces challenges due to the lower-than-expected energy density of sulfur and poor cycling life. This is due to the dissolution of intermediate charge/discharge products (lithium polysulfides, LiPSs) in the electrolyte, as well as the insulating nature of sulfur (S_8) and the discharge products (Li_2S_2 and Li_2S).[4,5] Additionally, LiPSs diffuse to the anode in a process called "polysulfide shuttling", exacerbating the problem by forming a passivating layer at the anode and blocking the transport of lithium ions.[5,6] Earlier efforts mainly focused on using conductive carbon materials as cathode hosts to trap LiPSs and mitigate the shuttle effect; however, weak van der Waals interactions with LiPSs eventually led to capacity loss over time.[7–9] Polar materials, including metal oxides (Al_2O_3, V_2O_5, TiO_2, Ti_4O_7, MnO_2, and MoO_2),[10–14] metal sulfides (TiS_2, FeS_2, MoS_2, and CoS_2),[10,11,14] metal-organic frameworks (MOFs),[14,15] and covalent organic frameworks (COFs),[16] have been used to confine polysulfides within

G. Valurouthu, M. Shekhirev, M. Anayee, R. (John) Wang, K. Matthews, T. Parker, R. W. Lord, D. Zhang, A. Inman, M. Downes, Y. Gogotsi
Department of Materials Science and Engineering, and A.J. Drexel Nanomaterials Institute
Drexel University
3141 Chestnut St., Philadelphia, PA 19104, USA
E-mail: gogotsi@drexel.edu

C. W. Ahn
Department of Nano-Structured Materials Research, and National NanoFab Center (NNFC)
291 Daehak-ro, Yuseong-gu, Daejeon 305–338, South Korea

V. Kalra
Robert Frederick Smith School of Chemical and Biomolecular Engineering
Cornell University
13 Ho Plaza, Ithaca, NY 14853, USA

I.-K. Oh
National Creative Research Initiative Center for Functionally Antagonistic Nano-Engineering, and Department of Mechanical Engineering
Korea Advanced Institute of Science and Technology (KAIST)
291 Daehak-ro, Yuseong-gu, Daejeon 34141, Republic of Korea
E-mail: ikoh@kaist.ac.kr

The ORCID identification number(s) for the author(s) of this article can be found under https://doi.org/10.1002/adfm.202404430

DOI: 10.1002/adfm.202404430

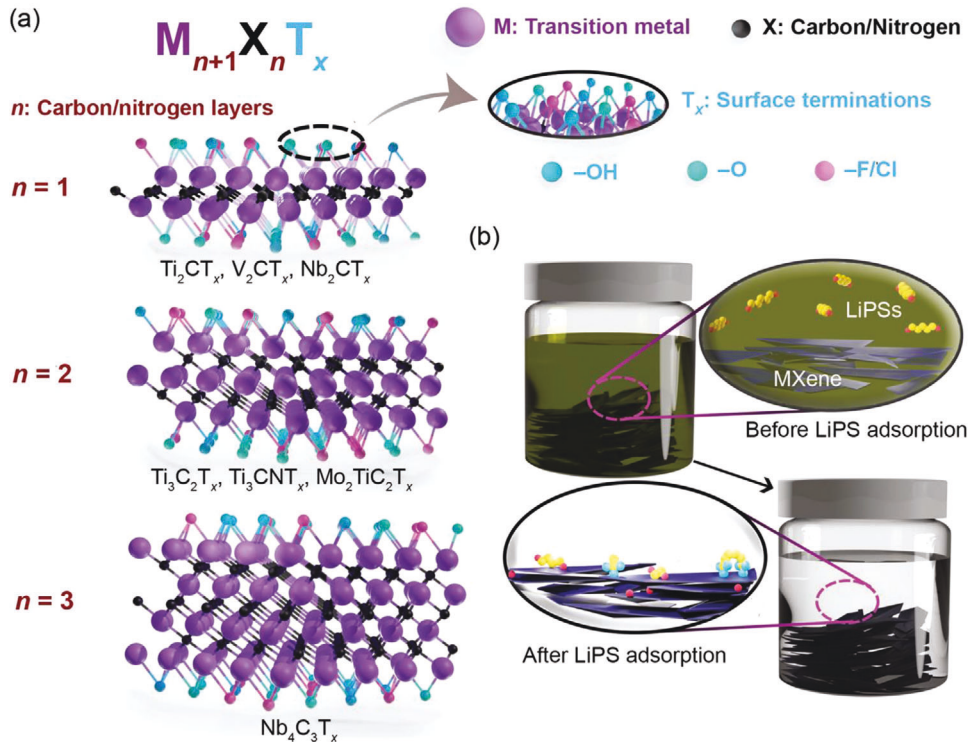

Figure 1. a) Representative atomic structures of MXenes employed in this study, with the inset showing the –O, –OH, and –F/Cl terminations. b) Schematic of the polysulfide adsorption test carried out in DME/DOL (1:1 by volume) solvent, with the inset showing the adsorption of polysulfides on the MXene flake surface.

cathodes chemically. Their intrinsic poor electrical conductivity resulted in sluggish reaction kinetics, reducing battery performance over time. This necessitated the use of conductive polar materials as cathode hosts for LSBs. In the past decade, conductive polar materials such as MXenes were investigated as sulfur cathode hosts and demonstrated stable long-term cycling.[17,18] This enhanced electrochemical performance was attributed to its oxide-like polar surface and metallic conductivity to address the polysulfide shuttle issue and sluggish kinetics.

Hence, MXenes, a family of 2D transition metal carbides, nitrides, and carbonitrides, emerged as a bifunctional solution for LSBs.[19–21] They are expressed in the form $M_{n+1}X_nT_x$, where M represents early transition metal, X represents carbon and/or nitrogen, *n* represents the number of carbon/nitrogen-atom-layers ranging from 1 to 4, and T_x represents surface terminations (**Figure 1**a). These materials have also demonstrated the potential to eliminate the extra use of current collectors,[22] conductive additives,[23] and binders[24] in Li-ion batteries, which can be extended to LSBs, offering innovative strategies to tackle the persistent polysulfide shuttling problem.[25–27] In recent years, $Ti_3C_2T_x$, Ti_2CT_x, Ti_3CNT_x, Mo_2CT_x, and V_2CT_x MXenes have been separately chosen for LSBs; however, the primary focus consistently placed on cell-level performance.[19–21,28,29] This shows the choice of MXenes has predominantly been empirical. Moreover, the MXene family is rapidly growing, with over 100 compositions theoretically predicted and 50 synthesized experimentally.[30,31] Therefore, it is crucial to gain a systematic understanding of the impact of the M layer, X layer, the number of M/X layers and surface terminations of this important family of materials on polysulfide adsorption and the associated mechanisms. Such studies have not been conducted before, and we believe it could help in fully utilizing their potential in enhancing the performance of LSBs.

Herein, we quantitatively compare the amount of LiPSs adsorbed by seven MXenes (Ti_2CT_x, $Ti_3C_2T_x$, Ti_3CNT_x, $Mo_2TiC_2T_x$, V_2CT_x, Nb_2CT_x, and $Nb_4C_3T_x$) consisting of three typical classes at the same time, that have four different transition metal outer-surface-layers (Ti, V, Nb, and Mo), two different X layers (C and CN), and three different structures (M_2CT_x, $M_3C_2T_x$, and $M_4C_3T_x$) covering the chemical space of most typical MXenes used in LSBs (Figure 1). We demonstrate, for the first time, that different MXene chemistries, when in contact with LiPSs, exhibit distinct polysulfide adsorption behaviors. The MXenes with the Ti outer layer, especially Ti_2CT_x, favored lithium, while the MXene with Mo outer layers, $Mo_2TiC_2T_x$, strongly favored sulfur redox reactions. Polysulfides adsorbed on all MXene surfaces eventually underwent oxidation to form thiosulfates and polythionate complexes, followed by a subsequent disproportionation into lower-order LiPSs (Li_2S_x, $x < 6$). We also show how variations in MXene chemistry strongly influence chemical interactions with LiPSs. These insights gained from the study hold the potential to assist researchers in selecting the most suitable MXene chemistry for designing efficient functional passive components tailored to the specific needs of next-generation LSBs.

2. Results

First, we quantified the polysulfide adsorption capacity of various MXene compositions employing UV-Vis spectroscopy. We then

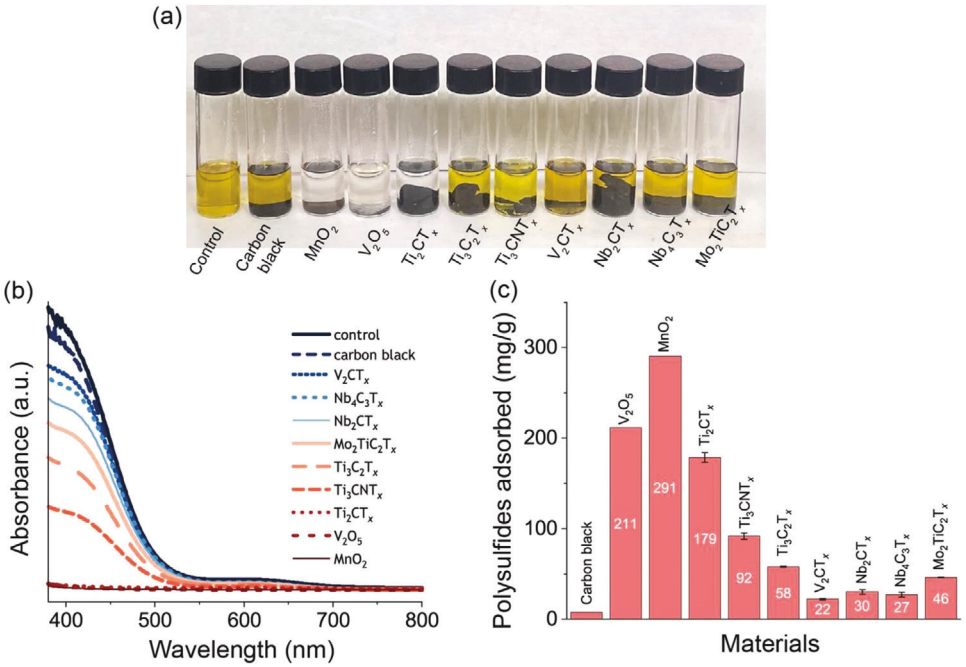

Figure 2. a) Photograph of the 2.5 mM Li_2S_6 solution after soaking with materials for 72 h (from left to right: control, carbon black, MnO_2, V_2O_5, Ti_2CT_x, $Ti_3C_2T_x$, Ti_3CNT_x, V_2CT_x, Nb_2CT_x, $Nb_4C_3T_x$, and $Mo_2TiC_2T_x$). b) UV–vis absorbance spectra of supernatant solution after soaking the materials. c) Calculated LiPS adsorption of materials.

developed adsorption isotherm and kinetic models to bring more insights into the LiPS adsorption process. We used inductively coupled plasma optical emission spectroscopy (ICP-OES) to measure the precise quantities of Li and S, regardless of their chemical states, to elucidate the type of adsorbed LiPS species. Finally, X-ray photoelectron spectroscopy (XPS) and Fourier transform infrared spectroscopy (FTIR) analyses were performed to study the influence of MXene chemistry on the polysulfide adsorption mechanism. These findings collectively lay the groundwork for our in-depth exploration and discussion of screening conductive MXenes for LSBs.

2.1. Quantitative Comparison of Polysulfide Adsorption

Seven MXene compositions, namely Ti_2CT_x, $Ti_3C_2T_x$, Ti_3CNT_x, $Mo_2TiC_2T_x$, V_2CT_x, Nb_2CT_x, and $Nb_4C_3T_x$, were selected based on differences in structure (# of atomic layers: M_2CT_x, $M_3C_2T_x$, and $M_4C_3T_x$), transition metal (M: Ti, V, Nb, and Mo), and core layers (X: C and CN) to cover the chemical space of most typical MXenes used in LSBs (Figure 1a). These MXenes were synthesized using a top-down wet chemical etching method utilizing HF or HF/HCl acid mixture from their respective MAX phase precursors (a representative MXene morphology is shown in Figure S1, Supporting Information), following procedures reported elsewhere (synthesis conditions are listed in Tables S1 and S2, Supporting Information).[32–34] The functional groups, such as –O, –OH, –F, and –Cl, displayed in Figure 1a, were introduced as a result of the aqueous etching process on the newly formed MXene surface. The ratio of different surface terminations depends on the specific etching conditions employed[35] and transition-metal atoms in the outer layer.[36] A 72 h polysulfide adsorption test was conducted to compare polysulfides adsorbed across MXene compositions.[11] MXenes were freeze-dried to maximize the accessible surface area (SEM images are shown in Figures S1c,d and S2, Supporting Information) and soaked in LiPS solution (Li_2S_6 in 1:1 by volume of 1,3-dioxolane (DOL) and dimethoxyethane (DME) solvent) as illustrated in Figure 1b. Li_2S_6 is chosen as a representative intermediate polysulfide, as it plays a significant role in polysulfide shuttling within the electrolyte of a typical LSB during the discharge process.[37]

The change in color of the polysulfide solution containing various MXenes serves as a convincing visual indicator of the amount of polysulfides adsorbed (**Figure 2a**). We also included well-established standard polysulfide adsorbents: carbon black, V_2O_5, and MnO_2. A darker residual LiPS solution signifies a higher concentration of LiPSs remaining in the solvent and less adsorption onto the material. Polysulfide solutions containing MnO_2, V_2O_5, and Ti_2CT_x turned utterly transparent, while Ti_3CNT_x, $Ti_3C_2T_x$, and $Mo_2TiC_2T_x$ displayed varying degrees of color change. V_2CT_x, Nb_2CT_x, and $Nb_4C_3T_x$ exhibited only a subtle shift in the color of their respective LiPS solutions, indicating a relatively weak LiPS adsorption. No perceptible color change was observed in the LiPS solution exposed to carbon black, aligning with prior research findings that suggest weaker physical adsorption.[11] The UV-Vis absorbance spectra of the supernatant following the adsorption test are displayed in Figure 2b. A higher absorbance value signifies a higher concentration of LiPS remaining in the supernatant. The LiPS concentration in the supernatant was determined using the linear dependence of absorbance at λ_{max} = ≈400 nm with the known concentrations of LiPSs in DME/DOL solvent (Figure S3, Supporting

Table 1. Estimated values of adsorption capacity and adsorbed species.

Material	UV-Vis method[a)]	ICP-OES method[b)]		Adsorbed species determined by XPS[c)]
	Li_2S_6 (mg g^{-1})	Li (mg g^{-1})	S (mg g^{-1})	
MnO_2	291, 124*	– 9*	– 20*	– PT*
V_2O_5	211, 16*	– 1*	– 2*	– PT*, T*
Ti_2CT_x	178	132	58	S_B, S_T, T, PT
Ti_3CNT_x	92	77	40	S_B, S_T, T, PT
$Ti_3C_2T_x$	58	81	76	S_B, S_T, T, PT
$Mo_2TiC_2T_x$	46	3	100	S_B, S_T, T, PT
Nb_2CT_x	30	2	4	S_B, S_T, T, PT
$Nb_4C_3T_x$	27	2	6	S_B, S_T, T, PT
V_2CT_x	22	2	1	S_B, S_T, PT, T
Carbon black	8, 22*	– 2*	– 21*	– S_B*, S_T*

*Reported in the literature[11]; [a)] estimated based on absorbance at 400 nm assuming Li_2S_6 is the only polysulfide species present in the supernatant; [b)] estimated in the materials; [c)] PT – polythionate complex, T – thiosulfate, S_B – bridge sulfur, S_T – terminal sulfur, and species labeled in orange are the predominant adsorption species.

Information), enabling estimation of the amount of polysulfides effectively adsorbed on the material. The adsorption process is a surface phenomenon directly proportional to a material's actual surface area and is usually normalized by surface area. However, the Brunauer–Emmett–Teller (BET) surface area of freeze-dried delaminated MXenes varied from 0.2 to 76 m^2 g^{-1} (Table S3, Supporting Information), with a value of 6 m^2 g^{-1} for $Ti_3C_2T_x$, which is significantly different from previously reported theoretical (242 m^2 g^{-1}) and experimental (23 m^2 g^{-1}) values.[38] The restacking of MXene flakes makes the adsorption of N_2 gas molecules on the flake surfaces challenging.[39] This renders the surface area of MXenes determined via the BET method unreliable. Consequently, there are notable disparities in adsorption capacity values when normalized by BET surface area, as demonstrated in Figure S4 (Supporting Information). Since BET surface area cannot provide an accurate basis for comparison, we opted for a definite parameter, mass, which is straightforward and can be readily determined. Under the selected equivalent conditions, carbon black, V_2CT_x, $Nb_4C_3T_x$, Nb_2CT_x, $Mo_2TiC_2T_x$, $Ti_3C_2T_x$, Ti_3CNT_x, Ti_2CT_x, V_2O_5, and MnO_2 estimated to adsorb 8, 22, 27, 30, 46, 58, 92, 179, 211, and 291 mg of polysulfides per gram of the material, respectively (Figure 2c, and **Table 1**). Among all the tested MXenes, the adsorption of LiPSs on Ti_2CT_x is comparable to MnO_2 and V_2O_5, which were reported to be strong polysulfide adsorption materials that can effectively prevent polysulfides from dissolving in electrolytes.[11] Ti_2CT_x exhibits the highest polysulfide adsorption, followed by Nb_2CT_x and V_2CT_x in M_2XT_x MXenes. Additionally, Ti_2CT_x and Ti_3CNT_x show superior polysulfide adsorption compared to $Ti_3C_2T_x$, despite the latter sharing a similar Ti outer layer and $M_3X_2T_x$ structure with the former materials, respectively. This suggests the influence of the M layer, X layer, and MXene structure on polysulfide adsorption, indicating that Ti is more effective than Nb and V, and N doping is beneficial. Additionally, the M_2XT_x structure is more efficient than the $M_3X_2T_x$ structure in trapping polysulfides.

2.2. Polysulfide Adsorption Isotherms and Kinetics

To estimate MXenes' maximum LiPS adsorption capacity and to understand the nature of the adsorption process, we used commonly chosen adsorption isotherm and kinetic models to fit for three most effective polysulfide adsorbing MXenes: Ti_2CT_x, Ti_3CNT_x, and $Ti_3C_2T_x$ as shown in **Figure 3**. Langmuir, Freundlich, and Liu isotherm models have been utilized to fit the adsorption isotherms to understand the interaction mechanism between LiPSs and MXene (Figure 3a).[40,41] The Langmuir model presumes single-layer adsorption with uniform adsorption sites, while the Freundlich model describes multilayer adsorption on heterogeneous surfaces. The Liu adsorption isotherm combines elements of both Langmuir and Freundlich models, assuming single-layer adsorption with variations in the adsorption site energies. Adjusted R^2 values (listed in Table S4, Supporting Information) of these fits indicate that Liu's adsorption isotherm model best describes the adsorption isotherms, suggesting that the MXene's surface has adsorption sites with varying energies and undergoes single-layer adsorption. Parameters such as maximum adsorption capacity (Q_o), heterogeneity of the site energy (n_s), and the equilibrium constants (K_L, K_F, and K_{Liu}) extrapolated from these models are presented in Table S4 (Supporting Information). Values of Q_o and n_s from the Liu adsorption model are 217 mg g^{-1} and 4.43 for Ti_2CT_x, 91 mg g^{-1} and 0.55 for $Ti_3C_2T_x$, and 129 mg g^{-1} and 2.00 for Ti_3CNT_x, respectively. The high value of maximum adsorption capacity of Ti_2CT_x can be attributed to its abundance of available adsorption sites per mass, likely due to its thin structure (a single layer of X compared to two layers of X in the case of $Ti_3C_2T_x$ and Ti_3CNT_x). Besides, the high value of n_s for Ti_2CT_x indicates a defect-rich surface, while $Ti_3C_2T_x$ features a lower n_s value, indicating a more uniform surface. These differences in the heterogeneity of the surface likely stem from the differences in the synthesis conditions of the materials, which have been reported for $Ti_3C_2T_x$.[32,42] The K_{Liu} signifies adsorption strength between the adsorbate and adsorbent, with the values of 17, 15, and 9 L g^{-1} for Ti_2CT_x, $Ti_3C_2T_x$, and Ti_3CNT_x, respectively (Table S4, Supporting Information). A higher K_{Liu} for Ti_2CT_x suggests a stronger interaction with polysulfides. Although Ti_3CNT_x has a defect-rich surface compared to $Ti_3C_2T_x$, its ≈42% higher Q_o compared to the latter can be attributed to its carbonitride (X) layer, alongside the defects.

The kinetic models provide insights into the mass transfer mechanism of the adsorption process (Figure 3b).[40,43] Pseudo-first-order and pseudo-second-order models were employed, which assume single-layer adsorption of adsorbate on a homogeneous adsorbent surface. The latter also assumes a chemical reaction between the adsorbate and adsorbent, which is the rate-limiting step. The parameters extrapolated from fitting these models, such as the equilibrium adsorption capacity (Q_e) and rate constants (k_1 and k_2), are listed in Table S5 (Supporting Information). Based on adjusted R^2 values, the pseudo-second-order model resulted in a better fit for all the MXenes tested, suggesting that polysulfides chemically interact with MXene resulting in chemisorption. The k_2 value for $Ti_3C_2T_x$ [25 g/(g·h)] was significantly higher than that of Ti_2CT_x [1.2 g/(g·h)] and Ti_3CNT_x [0.5 g/(g·h)], signifying that $Ti_3C_2T_x$ reaches equilibrium faster than the other two MXenes. This can be further correlated to the heterogeneity factor (n_s), which states that the more uniform

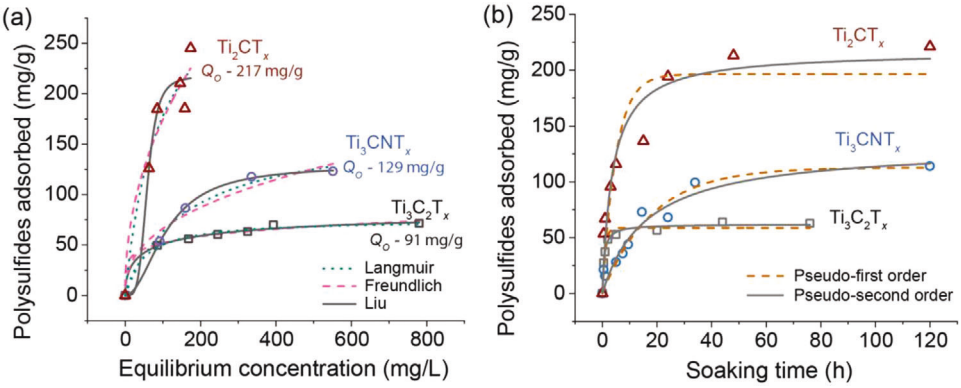

Figure 3. Lithium polysulfide adsorption on Ti-based MXenes. a) Adsorption isotherms of Li_2S_6 in DME/DOL for Ti_2CT_x, Ti_3CNT_x and $Ti_3C_2T_x$ subjected to 24 h adsorption tests were fitted using the Langmuir (dotted line), Freundlich (dashed line) and the Liu model (solid line). b) Polysulfide adsorption curves for Ti_2CT_x, Ti_3CNT_x, and $Ti_3C_2T_x$ were fitted using pseudo-first-order (dashed line) and pseudo-second-order kinetic models (solid line).

the surface, the faster the adsorption rate. Next, to deepen the understanding of the adsorption process's mechanism, we applied the intraparticle diffusion model (Q_t versus $t^{0.5}$) to fit the experimental kinetics data (Figure S5, Supporting Information).[43] This model assumes that the adsorption process occurs in several steps, including mass transfer from adsorbate to adsorbent, adsorbate binding to active sites, and diffusion within the adsorbent (also called intraparticle diffusion). Linear fit for all MXenes suggests polysulfide molecules undergo intraparticle diffusion within the MXene structure, which is considered one of the rate-limiting steps. This implies that MXene flakes are stacked to form few-layered structures despite freeze-drying the delaminated MXene single-layers (Figures S1c,d, and S2, Supporting Information). Especially, linear fit in the case of $Ti_3C_2T_x$ passes through the origin, indicating that the intraparticle diffusion is the sole rate-limiting step of the adsorption process, likely due to its uniform surface. It is worth noting that, in addition to variations in MXene chemistry, factors such as accessible surface area and defects or irregularities on the surface, which are often overlooked, play a role in polysulfide adsorption.

2.3. Quantitative Estimation of Li and S Atomic Concentration

The actual amount of S and Li remaining in the supernatant and adsorbed by the MXene following the adsorption test, was quantified using ICP-OES, as detailed in Table 1. This method allows for accurate quantification of S and Li, regardless of their chemical states, without being affected by complications related to unstable polysulfide species. The ratio of S and Li elements that remained in the MXene-soaked polysulfide solution after the adsorption test can help speculate the nature of adsorption species in greater detail (**Figure 4**; Figure S6, Supporting Information). All ratios represent the average of S and Li irrespective of their oxidation state. Specifically, the higher ratios (>4) may indicate a mixture of S_8 and various lithium polysulfide species. The atomic ratio of the supernatant of carbon black was five, which remained similar to that of the control, indicating that the initial polysulfide species did not undergo significant change upon adsorption on this material, which is consistent with previous literature (Figure S6, Supporting Information).[11] However, after individual adsorption tests with various MXene compositions, the S:Li atomic ratio of the supernatant varied from 7 to 23, deviating from the control. This implies that more sulfur remained in the supernatant, and MXenes selectively adsorbed more lithium. Due to an anomaly observed in the S/Li ratio of the material and supernatant following the $Mo_2TiC_2T_x$ adsorption test, we chose not to delve further into the discussion of ICP-OES data for this MXene (Figure S6b, Supporting Information). Except for $Mo_2TiC_2T_x$, the high S:Li atomic ratio in the supernatant further complemented the low values of S:Li atomic ratio (<0.6) within these materials, confirming their preference for Li (Figure 4). This preference can be attributed to the preferential intercalation of Li^+ ions between the MXene layers due to the O surface groups.[44,45] The S:Li atomic ratio of the polysulfides adsorbed on the MXenes shows varying trends depending on the 'M' (Ti_2CT_x < V_2CT_x < Nb_2CT_x) layer, 'X' (Ti_3CNT_x < $Ti_3C_2T_x$) layer and the structure (Ti_2CT_x < $Ti_3C_2T_x$). This further supports the role of the outer transition-metal layer, X layer, and the MXene structure in mediating the redox reactions between MXenes and the adsorbed species, which will be further discussed in Section 2.4. Ti-based MXenes have a higher content of Li (81–132 mg g^{-1})

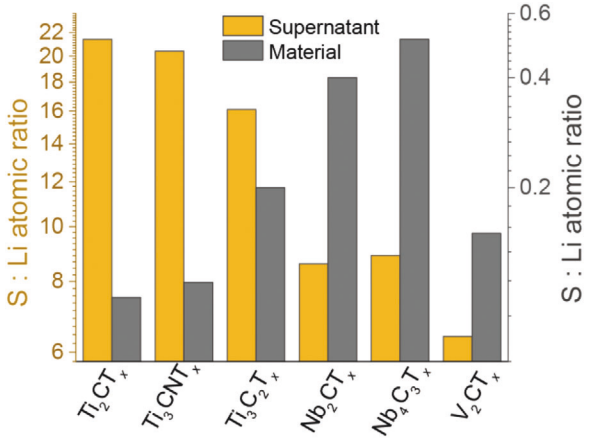

Figure 4. ICP-OES data of the sulfur to lithium atomic ratio of polysulfides remaining in the supernatant (yellow) and adsorbed on the MXene (grey) in log scale following a 72 h adsorption test.

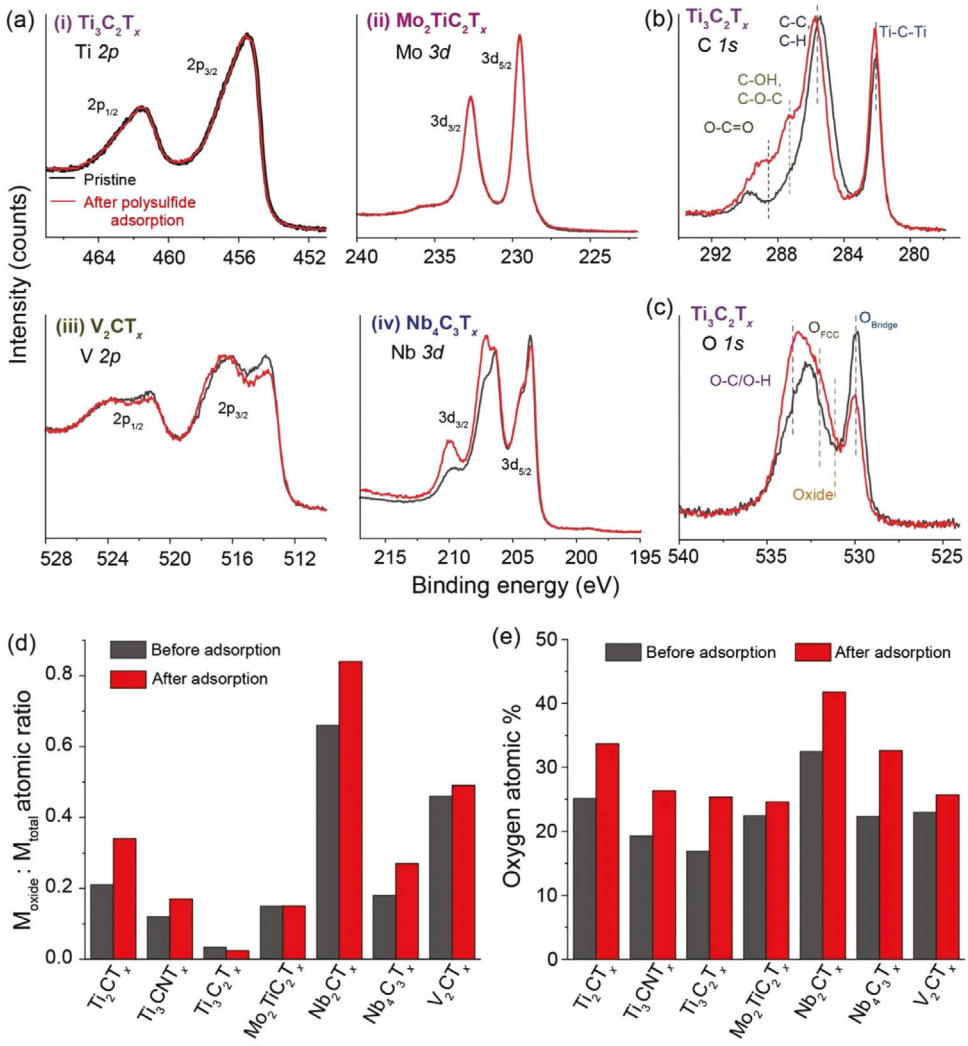

Figure 5. High-resolution XPS spectra of MXene aerogels before (black) and after (red) polysulfide adsorption. a) Spectra of outer-transition metal layer of MXenes i) Ti 2*p* of $Ti_3C_2T_x$, ii) Mo 3*d* of $Mo_2TiC_2T_x$, iii) V 2*p* of V_2CT_x, and iv) Nb 3*d* of $Nb_4C_3T_x$. b) Atomic ratio of metal oxide to total metal content (only the outer transition metal is considered) in the material. c) C 1*s* and d) O 1*s* spectra of $Ti_3C_2T_x$ and e) total oxygen content in the material before and after the adsorption test.

compared to other MXenes (2-3 mg g^{-1}). This is likely due to the selective adsorption of lithium influenced by the Ti outer metal layer and the subsequent preference of lithium-ion adsorption to form lithium multilayers on Li-adsorbed-MXene surfaces, as previously demonstrated for $Ti_3C_2T_x$.[45]

2.4. Interaction between LiPS and MXenes: Identification of Adsorbed Species

Any change in the surface species and changes in the oxidation state of the transition metal of MXenes, brought by chemical reactions with polysulfides, were investigated by XPS. First, the transition metal carbide (M-C-M) peak at ≈282 eV in C 1*s* spectra of materials confirmed the successful preparation of MXenes (Figures S7–S13, Supporting Information).[46,47] Ti 2*p* ($Ti_3C_2T_x$) and Mo 3*d* ($Mo_2TiC_2T_x$) spectra remained unchanged after the adsorption test, implying that polysulfide interactions with these MXenes did not bring any noticeable change in the chemical environment of outer transition metal layer. However, noticeable oxidation was observed in the outer transition metal spectra of the remaining tested MXenes (**Figure 5a**; Figures S7–S13, Supporting Information). This oxidation is characterized by an increase in peak intensity at higher binding energies and a decrease in intensity at lower binding energies. More stable $M_3C_2T_x$ and $M_4C_3T_x$ structures underwent less oxidation compared to the M_2CT_x structure (Figure 5b). For instance, the Ti^{4+} (oxide) to overall Ti content and $Nb^{4+/5+}$ to overall Nb content increased by ≈13 and 18% for Ti_2CT_x and Nb_2CT_x, respectively whereas this change is minimal (5% for Ti_3CNT_x and 9% for $Nb_4C_3T_x$) to none ($Mo_2TiC_2T_x$ and $Ti_3C_2T_x$) for $M_3C_2T_x$ and $M_4C_3T_x$ structures. Although V_2CT_x belongs to the M_2CT_x structure, very little oxidation (3% change) was observed for V_2CT_x. This could result from the enhanced chemical stability of V_2CT_x achieved through our optimized synthesis conditions, as reported previously.[34] It is evident that the oxidation of MXenes

during adsorption is influenced by both the chemical stability of the produced MXene and their inherent structural stability.

In the C 1*s* spectra of $Ti_3C_2T_x$, there was no significant change in the intensity or shift in the binding energy of the carbide peak (Ti-C-Ti) at ≈282 eV, confirming that the carbide structure remained intact even after the adsorption test (Figure 5c). However, there was an increase in the intensity of the peaks related to organic content at ≈284–290 eV. This may have been caused by the adsorption of residual DME/DOL solvent or their decomposition products on the surface of MXene. This trend was observed across all samples, where the atomic ratio of adventitious and/or organic carbon (≈284–290 eV) to carbide (≈282 eV) increased after adsorption (Figure S14, Supporting Information). Similarly, the O 2*p* spectra of all MXenes showed significant changes, indicating a chemical environment change of the oxygen surface groups after the adsorption test (Figures S7–S13, Supporting Information). Upon closer inspection of $Ti_3C_2T_x$, it was found that there was a decrease in the intensity of –O surface groups at low binding energy (≈529 eV) and an increase in O contribution at higher binding energies (Figure 5d). This was observed across all MXene compositions and can be attributed to 1) polysulfides forming O_{MXene}-S_{LiPS}/Li_{LiPS} bonds and 2) the adsorption of solvent residue (O-H/O-C) (Figures S9–S12, Supporting Information).

It was also observed that oxygen content in all the MXenes increased following adsorption, indicating that extra oxygen came from the solvent (Figure 5e). However, the significant increase in organic oxygen and carbon content for Nb_2CT_x (>Ti_2CT_x > V_2CT_x) and $Nb_4C_3T_x$ following the adsorption indicates a strongly adsorbed layer of solvent on these surfaces compared to other tested MXenes (Figure 5e; Figure S14, Supporting Information). This suggests that the interactions of MXene with solvent depend on the MXene chemistry, especially the transition metal identity in the outer layer and, additionally, the chemical stability of the MXene prepared. In addition, solvent adsorption on MXenes also depends on the X layer, where a higher organic oxygen/carbon content was found in Ti_3CNT_x than in $Ti_3C_2T_x$. Our XPS observations further confirmed that fluorine and chlorine terminations did not participate in adsorption (Figure S7c and d, Supporting Information), agreeing with previous computational studies on $Ti_3C_2T_2$.[48] Nevertheless, these terminations influence the concentration of oxygen terminations, potentially affecting the extent to which polysulfides interact with MXenes.

S 2*p* spectra of MXenes collected after the adsorption test revealed four doublet chemical environments (**Figure 6a**). These correspond to terminal S (S_T, −1 oxidation state) at ≈162.5/163.7 eV, bridging S (S_B, 0 oxidation state) at 164.2/165.4 eV, thiosulfate (+4 oxidation state) at 167.3/168.5 eV and polythionate (+5 oxidation states) sulfur species at 168.8/170.0 eV.[13] The presence of these four sulfur species suggests that all tested MXenes physically bound polysulfides. The O surface groups chemically interact with polysulfides to form thiosulfates and polythionates.[17,18] It is important to note that O surface groups are critical for the chemisorption of polysulfides. The distribution of these adsorption species was distinctive for different MXenes (Figure 6b). Although titanium is in the outer transition metal layer, Ti_2CT_x predominantly contained polythionate and thiosulfate species compared to $Ti_3C_2T_x$ and Ti_3CNT_x (Table 1, Figure 6b), due to the high oxygen content on its surface as shown by XPS (Figure 5e). In contrast, Nb_2CT_x and $Nb_4C_3T_x$ have similar distributions of sulfur species, possibly due to shared characteristics, like a niobium transition metal outer layer and heavily oxide-covered surface (Figure 5e). Interestingly, $Mo_2TiC_2T_x$ has equal proportions (≈30%) of S_T, S_B, and polythionate species, with a ≈10% contribution from thiosulfate species (Figure 6b). The S 2*p* spectrum also shifted toward lower binding energy than $Ti_3C_2T_x$, specifically the S_T shifted by ≈0.8 eV. This shift suggests the presence of low-order polysulfides (Li_2S_x, where $1 \leq x \leq 4$), indicating a reaction between initial polysulfides and thiosulfates formed upon adsorption to yield polythionate complexes with longer sulfur chains and low-order polysulfide species. This observation implies a significant degree of polysulfide conversion on the $Mo_2TiC_2T_x$ surface. The effect of the 'X' layer on polysulfide conversion does not seem obvious, but thiosulfate to polythionate conversion is higher in $Ti_3C_2T_x$ compared to Ti_3CNT_x. This can be attributed to the greater electronegativity of the carbonitride core compared to the carbide core.[49] As a result, the surface charge becomes slightly more negative, which selectively prefers Li over S. This is consistent with the Li/Ti and S/Ti atomic ratios (Table S6, Supporting Information). Overall, the XPS analysis shows that the chemical trapping of polysulfides depends particularly on the terminations while the extent of selective adsorption and polysulfide conversion depends on the unique chemistry of individual MXenes, particularly the transition metal identity, X layer, and oxygen coverage on the MXene surface.

To gain a better understanding of the chemical bonds formed between polysulfides and O surface groups of MXenes, FTIR was performed on materials before and after the adsorption test (Figure 6c; Figure S15, Supporting Information). For all MXenes before adsorption, two distinct vibration peaks were observed: the metal-carbide (M—C) bond within the range of 450–350 cm^{-1} and the metal-oxide (M—O) bond within the range of 650–550 cm^{-1}. However, a broad absorption band at 600–450 cm^{-1} was found upon polysulfide adsorption.[50,51] This broad absorption band corresponds to the overlap of S–S (S_x^{2-}, $2 \leq x \leq 8$) and M—O—S bonds, which are supposed to be at 500–450 and 600–400 cm^{-1}, respectively, confirming the M–O–S bond formation between –O terminations (and/or oxides produced from harsh etching conditions) of MXenes and polysulfides. This is further supported by a small shift of the resonant peak (126 cm^{-1}) to a higher wavenumber and the A_{1g}(C) peak (728 cm^{-1}) to a lower wavenumber in the Raman spectrum of $Ti_3C_2T_x$, indicating altered surface chemistry following the adsorption test (Figure S16, Supporting Information).[52] Two distinct and sharp FTIR bands of S–S (S_x^{2-}, $2 \leq x \leq 8$) bond (at 520 cm^{-1}) and M—O—S bond (at 550 cm^{-1}) were observed for $Mo_2TiC_2T_x$, indicating more S_B and thiosulfate/polythionate species, respectively, in agreement with the XPS data.

3. Discussion

Our study involving seven distinct MXenes with variations in transition metal identity (M layer), X layer, and structure shows that all selected MXenes have the potential to mitigate the shuttle effect. A combination of spectroscopic analyses (UV–vis, ICP-OES, XPS, and FTIR) confirmed polysulfide adsorption is strongly affected by MXene structure, transition metal identity

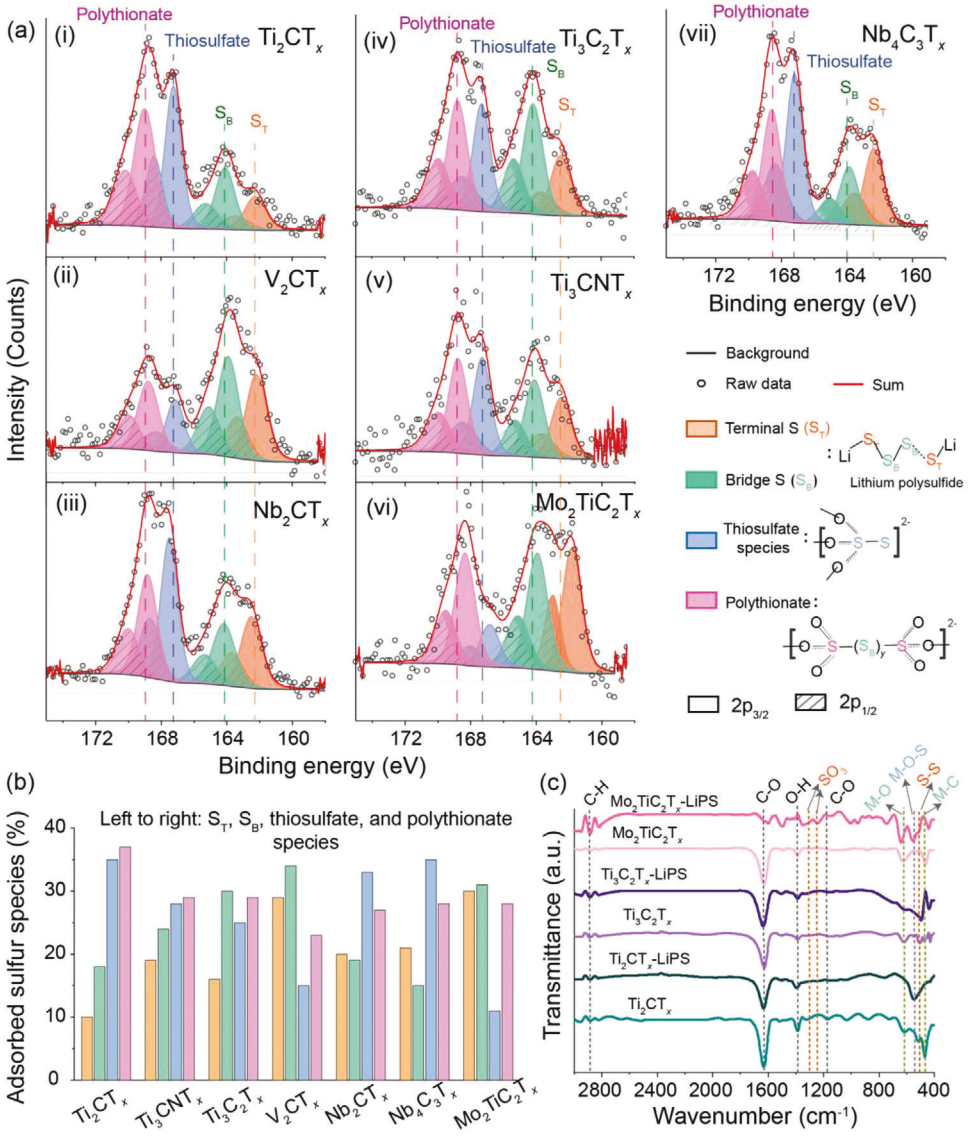

Figure 6. a) High-resolution S 2*p* XPS spectra of MXene aerogels subjected to polysulfide adsorption test, i) Ti_2CT_x, ii) V_2CT_x, iii) Nb_2CT_x, iv) $Ti_3C_2T_x$, v) Ti_3CNT_x, vi) $Mo_2TiC_2T_x$, and vii) $Nb_4C_3T_x$. b) Atomic % of adsorbed sulfur species with respect to the total sulfur content adsorbed on MXenes. c) FTIR spectroscopy of MXenes before and after being subjected to the adsorption test.

in the outer transition metal layer, surface terminations, and defects/oxide coverage on the surface. While Ti_2CT_x has a high adsorption capacity due to its thin structure (Figure 2), the adsorption kinetics were faster for $Ti_3C_2T_x$, possibly due to its homogeneous surface with fewer defects (Figure 3). However, the same structure-property relationship cannot be extended to Nb_2CT_x and $Nb_4C_3T_x$ MXenes, potentially due to the oxide coverage obscuring the intrinsic nature of the adsorption mechanism. On the other hand, Nb-based MXenes strongly interact with the solvent, forming a thick solid electrolyte interphase (SEI) layer on their surface, possibly due to the reactive Nb outer layer (Figure 5e; Figure S14, Supporting Information). When correlating the adsorption property to the transition metal identity in M_2XT_x MXenes, Ti_2CT_x demonstrates a preference for Li-ion adsorption followed by V_2CT_x while Nb_2CT_x shows both high reactivity with the solvent and a preference for sulfur over Li. Moving on to $M_3X_2T_x$ MXenes, those with Ti-outer-layer prefer lithium, whereas Mo-outer-layer ($Mo_2TiC_2T_x$) favors sulfur due to the strong adsorption preference and/or surface redox mediation of transition metal in the outer-transition metal layer (Figure 4).

Ti_2CT_x, Ti_3CNT_x, and $Ti_3C_2T_x$ have been previously demonstrated to chemically interact with polysulfides via thiosulfate-polythionate conversion and Lewis acid-base interactions, forming O_{MXene}–S_{LiPS} and Ti_{MXene}–S_{LiPS} bonds, respectively.[17,18] In contrast to our observed dependence of structure and X-layer on adsorption properties, these MXenes have been reported to exhibit similar electrochemical performance (Table S7, Supporting Information).[17,18] This could be attributed to the heavy oxide coverage on the material surface resulting from the synthesis conditions at that time. These factors might have obscured the

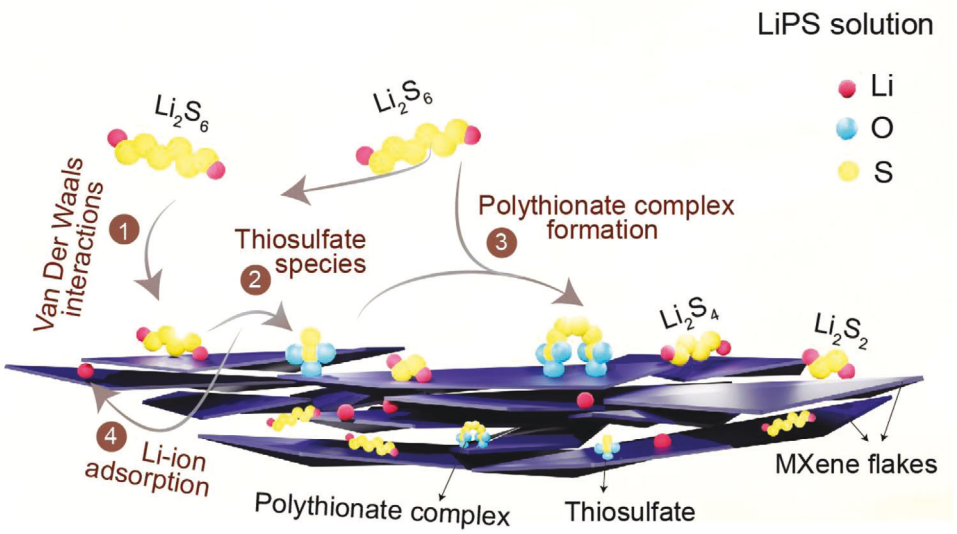

Figure 7. Schematic illustration of the adsorption mechanism of polysulfides on the surface of MXenes.

structure- and X-layer-dependent electrochemical performance. This agrees with our structure-property observations on Nb-based MXenes (Figure 6). It is important to note that the continually evolving MXene synthesis protocols aim to enhance MXene chemical stability by reducing defect concentration and suppressing oxide formation. As a result, some previously observed adsorption behaviors have changed. For instance, V_2CT_x, which is known to be highly susceptible to oxidation, like several other M_2CT_x structures, has undergone minimal oxidation (Figure 5b). This is correlated to its improved synthesis conditions that have produced a chemically stable V_2CT_x.[34] In the present study on MXenes prepared following our recent synthesis protocols,[32–34] the polysulfide adsorption followed thiosulfate–polythionate conversion and remained the same for all the MXenes due to the presence of O surface groups (Figure 6). Chemically and structurally stable MXenes such as $Ti_3C_2T_x$ and $Mo_2TiC_2T_x$ exhibited chemical interactions with polysulfides (thiosulfate/polythionate redox mediation) without significant changes in the oxidation state of transition metal (Figure 5b). Therefore, MXene's oxidation stability against LiPS and/or solvent also depends on the chemical and structural stability of the MXene produced. We also found chemical bonding between polysulfides and MXenes to be dependent on the O surface groups and/or oxide content in the material (Figure 6b). However, the extent of thiosulfate to polythionate conversion strongly depends on the transition metal identity, surface oxide coverage, and, to some extent, the X layer composition.

Based on our systematic investigation, we hypothesize polysulfide adsorption on MXenes follows four steps, as illustrated in **Figure 7**. First, polysulfides (S_x^{2-}, where $4 \leq x \leq 8$) physically adsorb on the MXene surface through van der Waals interactions. Then, the adsorbed polysulfides undergo redox reactions with the –O terminations to form thiosulfate species ($S_2O_3^{2-}$). These adsorption species act as anchors to capture 'higher-order' polysulfides (S_x^{2-}, where $x \geq 4$) and further mediate polysulfide redox reactions forming surface-bound polythionate complexes [$^-O_3S-(S)_y-SO_3^-$; where $y \geq 0$] and low-order polysulfides (S_x^{2-}, where $x \leq 4$). Lastly, Li^+ ions adsorb between the MXene layers and/or chemically react to form —O—Li bonds. For a more comprehensive understanding of MXene's chemistry influence on polysulfide adsorption, future research should emphasize optimizing MXene synthesis methods to produce chemically stable MXenes with consistent and controlled chemistry. Follow-up electrochemical studies employing advanced in-situ techniques such as X-ray absorption, infrared and Raman spectroscopy, as well as validations from Density Functional Theory (DFT) investigations, could advance our understanding of MXenes' mitigation of polysulfide shuttle, thereby advancing their application in Li-S batteries.

4. Conclusions

We systematically investigated seven MXenes, encompassing the chemical diversity of the most common MXenes, as polar conductive polysulfide adsorbents for potential applications in Li-S batteries. Multimodal analysis revealed a wide range of polysulfide adsorption, up to 217 mg per gram of material, depending on the MXene composition, soaking time, and polysulfide concentration. Specifically, the polysulfide adsorption for V_2CT_x, $Nb_4C_3T_x$, Nb_2CT_x, $Mo_2TiC_2T_x$, $Ti_3C_2T_x$, Ti_3CNT_x, and Ti_2CT_x were 22, 27, 30, 46, 58, 92, and 179 mg per gram of the material, respectively, under a fixed polysulfide concentration and soaking time. Several factors, such as accessible surface area and adsorption site energies, which are further controlled by the MXene structure and its synthesis process, play a critical role in polysulfide adsorption. Regardless of MXene composition, the polysulfide adsorption mechanism followed the thiosulfate/polythionate redox mediation pathway attributed to oxygen terminations intrinsic to all MXenes prepared by wet etching of MAX phase precursors. However, the extent of polysulfide redox reactions and selective adsorption between Li^+ and S_x^{2-} of the polysulfides depended on the MXene chemistry, including transition metal layers, X layer, and defects or oxide content. $Mo_2TiC_2T_x$ potentially retained high sulfur content through effective thiosulfate/polythionate redox mediation. Conversely, Ti-based MXenes have high lithium content (81–132 mg g^{-1}) and showed

selectivity for Li^+ ions of the polysulfides. There is potential for Mo-based MXenes as cathode hosts/additives to inhibit the shuttle effect and for Ti-based MXenes as interlayer and separator coatings to facilitate selective Li^+ ion transport to improve the overall performance of the LSBs. This new understanding emphasizes the importance of application-dependent MXene selection. It also opens up the possibility of utilizing Ti-based MXenes for various applications, such as the selective extraction and transportation of Li ions in desalination and/or Li-based batteries.

5. Experimental Section

The Experimental Section and any associated references are available in the Supporting Information.

Supporting Information

Supporting Information is available from the Wiley Online Library or from the author.

Acknowledgements

This work was supported by the DOE SBIR program DE-SC0021521 and the DOE-EERE program DE-EE0009646, both as subcontracts to Giner, Inc. The authors acknowledge support from the National Research Foundation of Korea (NRF) grants funded by the Korean government ([MSIT] [no. RS-2023-0030252] and [MEST] [no. NRF-2021M3H4A1A03047333]). T.H. acknowledges support from the US National Science Foundation under M-STAR CCI (CHE-2318105). V.K. acknowledges the NSF-PFI-TT program (1919177). The authors thank the KAIST Analysis Center for Research Advancement (KARA) for the use of the characterization facility. The authors thank Sanghee Nam and Teng Zhang for their help in conducting the study.

Conflict of Interest

The authors declare no conflict of interest.

Author Contributions

Y.G. initiated and directed the study. Y.G., I.K.O., and C.W.A. provided the resources to conduct the study. G.V. conceived the original research idea and conducted most of the measurements and analysis. M.S., K.M., R.W.L., D.Z., M.D., and A.I. conducted materials synthesis. T.H. contributed to part of the spectroscopic measurements. M.A. and T.H. contributed to the data processing. R.W. and V.K. provided the mechanism idea. All authors contributed to the discussion and revising of this manuscript. All data used in this study are available from the corresponding authors upon reasonable request.

Data Availability Statement

The data that support the findings of this study are available from the corresponding author upon reasonable request.

Keywords

adsorption mechanism, Li-S battery, MXenes, polysulfide adsorption, thiosulfates/polythionates

Received: March 13, 2024
Revised: May 18, 2024
Published online:

[1] B. Dunn, H. Kamath, J. M. Tarascon, *Science*. **2011**, *334*, 928.
[2] J. Sun, T. Wang, Y. Gao, Z. Pan, R. Hu, J. Wang, *InfoMat*. **2022**, *4*, e12359.
[3] R. Fang, S. Zhao, Z. Sun, D. W. Wang, H. M. Cheng, F. Li, *Adv. Mater.* **2017**, *29*, 1606823.
[4] A. Manthiram, Y. Fu, Y. S. Su, *Acc. Chem. Res.* **2013**, *46*, 1125.
[5] L. Qie, C. Zu, A. Manthiram, *Adv. Energy Mater.* **2016**, *6*, 1502459.
[6] R. Cao, W. Xu, D. Lv, J. Xiao, J.-G. Zhang, *Adv. Energy Mater.* **2015**, *5*, 1402273.
[7] Y. Yang, G. Zheng, Y. Cui, *Chem. Soc. Rev.* **2013**, *42*, 3018.
[8] X. Ji, K. T. Lee, L. F. Nazar, *Nat. Mater.* **2009**, *8*, 500.
[9] G. Zhou, L. Li, C. Ma, S. Wang, Y. Shi, N. Koratkar, W. Ren, F. Li, H. M. Cheng, *Nano Energy*. **2015**, *11*, 356.
[10] X. Liu, J.-Q. Huang, Q. Zhang, L. Mai, *Adv. Mater.* **2017**, *29*, 1601759.
[11] D. S. Wu, F. Shi, G. Zhou, C. Zu, C. Liu, K. Liu, Y. Liu, J. Wang, Y. Peng, Y. Cui, *Energy Storage Mater.* **2018**, *13*, 241.
[12] X. Liang, C. Y. Kwok, F. Lodi-Marzano, Q. Pang, M. Cuisinier, H. Huang, C. J. Hart, D. Houtarde, K. Kaup, H. Sommer, T. Brezesinski, J. Janek, L. F. Nazar, *Adv. Energy Mater.* **2016**, *6*, 1501636.
[13] X. Liang, C. Hart, Q. Pang, A. Garsuch, T. Weiss, L. F. Nazar, *Nat. Commun.* **2015**, *6*, 1.
[14] J. Balach, J. Linnemann, T. Jaumann, L. Giebeler, *J. Mater. Chem. A.* **2018**, *6*, 23127.
[15] Y. Zheng, S. Zheng, H. Xue, H. Pang, *J. Mater. Chem. A.* **2019**, *7*, 3469.
[16] B. Hu, J. Xu, Z. Fan, C. Xu, S. Han, J. Zhang, L. Ma, B. Ding, Z. Zhuang, Q. Kang, X. Zhang, *Adv. Energy Mater.* **2023**, *13*, 2203540.
[17] X. Liang, A. Garsuch, L. F. Nazar, *Angew. Chemie Int. Ed.* **2015**, *54*, 3907.
[18] X. Liang, Y. Rangom, C. Y. Kwok, Q. Pang, L. F. Nazar, *Adv. Mater.* **2017**, *29*, 1603040.
[19] Q. Zhao, Q. Zhu, Y. Liu, B. Xu, *Adv. Funct. Mater.* **2021**, *31*, 2100457.
[20] C. Zhang, L. Cui, S. Abdolhosseinzadeh, J. Heier, *InfoMat*. **2020**, *2*, 613.
[21] Y. Wang, T. Guo, E. Alhajji, Z. Tian, Z. Shi, Y.-Z. Zhang, H. N. Alshareef, *Adv. Energy Mater.* **2023**, *13*, 2202860.
[22] Z. Wang, C. Wei, H. Jiang, Y. Zhang, K. Tian, Y. Li, X. Zhang, S. Xiong, C. Zhang, J. Feng, *Adv. Mater.* **2024**, *36*, 2306015.
[23] L. Cui, C. (John) Zhang, *Chem*. **2023**, *5*, 100110.
[24] C. Zhang, W. Zhao, S. H. Park, T. Guo, S. Deng, A. Seral-Ascaso, M. Si, R. Grissa, S. Barwich, V. Nicolosi, *Adv. Funct. Mater.* **2023**, *33*, 2213860.
[25] H. Tang, W. Li, L. Pan, K. Tu, F. Du, T. Qiu, J. Yang, C. P. Cullen, N. McEvoy, C. (John) Zhang, *Adv. Funct. Mater.* **2019**, *29*, 1901907.
[26] J. Song, D. Su, X. Xie, X. Guo, W. Bao, G. Shao, G. Wang, *ACS Appl. Mater. Interfaces*. **2016**, *8*, 29427.
[27] Y. Dong, S. Zheng, J. Qin, X. Zhao, H. Shi, X. Wang, J. Chen, Z. S. Wu, *ACS Nano*. **2018**, *12*, 2381.
[28] Y. Zhang, C. Ma, W. He, C. Zhang, L. Zhou, G. Wang, W. Wei, *Prog. Nat. Sci.: Mater. Int.* **2021**, *31*, 501.
[29] Z. Xiao, Z. Li, X. Meng, R. Wang, *J. Mater. Chem. A.* **2019**, *7*, 22730.
[30] M. Downes, C. E. Shuck, R. W. Lord, M. Anayee, M. Shekhirev, R. J. Wang, T. Hryhorchuk, M. Dahlqvist, J. Rosen, Y. Gogotsi, *ACS Nano*. **2023**, *17*, 17158.
[31] B. Anasori, Y. Gogotsi, *Graphene and 2d Mater.* **2023**, *8*, 39.
[32] T. S. Mathis, K. Maleski, A. Goad, A. Sarycheva, M. Anayee, A. C. Foucher, K. Hantanasirisakul, C. E. Shuck, E. A. Stach, Y. Gogotsi, *ACS Nano*. **2021**, *15*, 6420.

[33] M. Han, C. E. Shuck, R. Rakhmanov, D. Parchment, B. Anasori, C. M. Koo, G. Friedman, Y. Gogotsi, *ACS Nano*. **2020**, *14*, 5008.
[34] K. Matthews, T. Zhang, C. E. Shuck, A. Vahid Mohammadi, Y. Gogotsi, *Chem. Mater.* **2022**, *34*, 499.
[35] M. A. Hope, A. C. Forse, K. J. Griffith, M. R. Lukatskaya, M. Ghidiu, Y. Gogotsi, C. P. Grey, *Phys. Chem. Chem. Phys.* **2016**, *18*, 5099.
[36] V. Kamysbayev, A. S. Filatov, H. Hu, X. Rui, F. Lagunas, D. Wang, R. F. Klie, D. V. Talapin, *Science*. **2020**, *369*, 979.
[37] R. Liu, Z. Wei, L. Peng, L. Zhang, A. Zohar, R. Schoeppner, P. Wang, C. Wan, D. Zhu, H. Liu, Z. Wang, S. H. Tolbert, B. Dunn, Y. Huang, P. Sautet, X. Duan, *Nature*. **2024**, *626*, 98.
[38] M. R. Lukatskaya, S. Kota, Z. Lin, M. Q. Zhao, N. Shpigel, M. D. Levi, J. Halim, P. L. Taberna, M. W. Barsoum, P. Simon, Y. Gogotsi, *Nat. Energy*. **2017**, *2*, 17105.
[39] J. Rouquerol, P. Llewellyn, F. Rouquerol, *Stud. Surf. Sci. Catal.* **2007**, *160*, 49.
[40] É. C. Lima, M. A. Adebayo, F. M. Machado, *Carbon Nanostructures in Carbon Nanomaterials as Adsorbents for Environmental and Biological Applications* **2015**, pp. 33–69.
[41] Q. Zhao, M. Seredych, E. Precetti, C. E. Shuck, M. Harhay, R. Pang, C. X. Shan, Y. Gogotsi, *ACS Nano*. **2020**, *14*, 11787.
[42] M. Alhabeb, K. Maleski, B. Anasori, P. Lelyukh, L. Clark, S. Sin, Y. Gogotsi, *Chem. Mater.* **2017**, *29*, 7633.
[43] J. Wang, X. Guo, *J. Hazard. Mater.* **2020**, *390*, 122156.
[44] O. Mashtalir, M. Naguib, V. N. Mochalin, Y. Dall'Agnese, M. Heon, M. W. Barsoum, Y. Gogotsi, *Nat. Commun.* **2013**, *4*, 1716.
[45] Y. Xie, M. Naguib, V. N. Mochalin, M. W. Barsoum, Y. Gogotsi, X. Yu, K. W. Nam, X. Q. Yang, A. I. Kolesnikov, P. R. C. Kent, *J. Am. Chem. Soc.* **2014**, *136*, 6385.
[46] L. Å. Näslund, I. Persson, *Appl. Surf. Sci.* **2022**, *593*, 153442.
[47] M. Saraf, B. Chacon, S. Ippolito, R. W. Lord, M. Anayee, R. Wang, A. Inman, C. E. Shuck, Y. Gogotsi, *Adv. Funct. Mater.* **2024**, *34*, 2306815.
[48] D. Wang, F. Li, R. Lian, J. Xu, D. Kan, Y. Liu, G. Chen, Y. Gogotsi, Y. Wei, *ACS Nano*. **2019**, *13*, 11078.
[49] T. Zhang, C. E. Shuck, K. Shevchuk, M. Anayee, Y. Gogotsi, *J. Am. Chem. Soc.* **2023**, *145*, 22374.
[50] S. Arunmetha, N. R. Dhineshbabu, A. Kumar, R. Jayavel, *J Mater Sci Mater Electron.* **2021**, *32*, 28382.
[51] C. Dillard, A. Singh, V. Kalra, *J. Phys. Chem. C.* **2018**, *122*, 18195.
[52] A. Sarycheva, Y. Gogotsi, *Chem. Mater.* **2020**, *32*, 3480.